Experimental realization of an approximate transpose operation for qutrit systems using a structural physical approximation

Hyang-Tag Lim,[1,*] Yong-Su Kim,[1,†] Young-Sik Ra,[1] Joonwoo Bae,[2,‡] and Yoon-Ho Kim[1,§]
[1]*Department of Physics, Pohang University of Science and Technology (POSTECH), Pohang 790-784, Korea*
[2]*Center for Quantum Technologies, National University of Singapore, 3 Science Drive 2, Singapore 117543*
(Received 31 August 2012; published 24 October 2012)

Although important for detecting entanglement, the transpose operation cannot be directly realized in laboratory because it is a nonphysical operation. It is, however, possible to find an approximate transpose operation using the method known as the structural physical approximation (SPA); recently, SPA-based implementations of the transpose and partial transpose have been demonstrated for a single-qubit [Phys. Rev. A **83**, 020301(R) (2011)] and an entangled two-qubit system [Phys. Rev. Lett. **107**, 160401 (2011)]. In this work, we expand SPA-transpose to a three-dimensional quantum system: a qutrit. The photonic qutrit state is encoded in the polarization, and path degrees of freedom of a single-photon and the SPA-transpose operation, which is based on measurement and preparation of quantum states, is implemented with linear optics. Our work paves the way toward entanglement detection for higher-dimensional quantum systems.

DOI: 10.1103/PhysRevA.86.042334 PACS number(s): 03.67.Bg, 03.65.Ud, 42.50.Ex

The transpose operation is of great importance in quantum information theory as it can be used for detecting useful entanglement: According to the Peres-Horodecki criteria, separable states give only positive eigenvalues after the partial transposition [1–3]. However, since the transpose is not a *completely positive* operation [2], it cannot be a physical quantum operation. In other words, it is fundamentally impossible to implement the transpose operation in the laboratory for detecting entanglement.

Instead, structural physical approximation (SPA), a systematic approximation to positive maps, has been proposed for the direct experimental entanglement detection in Ref. [4]. In SPA, an original nonphysical operation (such as transpose) is admixed with a precise amount of white noise to construct an approximate operation which is *completely positive*, such that the newly constructed approximate operation is a physical quantum operation. Since the added white noise is isotropic, the approximate operation can retain important properties of the original nonphysical operation. SPA proposed in Ref. [4] is still technically difficult to implement as collective measurement, requiring coherent quantum operations over multiple identically prepared quantum systems and quantum memory, is assumed for spectrum estimation. Recently, it has been conjectured that SPA to a positive map is entanglement breaking [5], meaning that for those maps that fulfill the conjecture, their SPA's can be realized with measurement and preparation of quantum states [6]. Thus, realization of the SPA operation becomes much simpler and feasible as it can be implemented with quantum operations (SPA of transpose, SPA of inversion, identity, and depolarization) over individual quantum systems.

To date, SPA operations have been implemented for the single-qubit and two-qubit systems only. In Ref. [7], SPA of the transpose operation (SPA-T) for a photonic qubit is reported. Here, the optimal approximate transpose operation for a qubit is implemented by SPA based on measurement and preparation of the photonic qubit using linear optics. Also, recently, SPA of the partial transpose operation (SPA-PT) for a two-qubit system has been experimentally demonstrated [8]. In Ref. [8], SPA-PT was realized linear optically assuming local operation and classical communication (LOCC) by using the fact that SPA-PT can be decomposed into a convex combination of local operations on individual subsystems [9].

Recently, communication of quantum information encoded in d-dimensional quantum systems, qudits, has attracted much attention [10–16]. Since Peres-Horodecki criteria can be applied to entangled qudits, SPA-PT could enable straightforward entanglement detection in high-dimensional quantum systems. In this work, as a step toward this direction, we report a linear optical experimental realization of SPA-T based on measurement and preparation of quantum states for a photonic three-dimensional quantum system (qutrit). The experimentally implemented SPA-T exhibits excellent agreement with the ideal SPA-T, as evidenced in the high process fidelity between the ideal quantum operation and the experimentally reconstructed quantum operation.

Let us begin by briefly introducing the theoretical background of SPA based on the measurement and preparation of quantum states [5]. The key idea of SPA is that one admixes a precise amount of white noise to a nonphysical operation Λ so that the approximate operation $\widetilde{\Lambda}$ is *positive* and *completely positive*, i.e., $\widetilde{\Lambda}$ can now be realized as it is a physical quantum operation. The approximate operation $\widetilde{\Lambda}$ can thus be written as

$$\widetilde{\Lambda} = (1-p)\Lambda + pD, \tag{1}$$

where $0 \leqslant p \leqslant 1$ and the contraction map $D[\rho] = I_d/d$ (I_d is a d-dimensional identity matrix) transforms the quantum state ρ into the maximally mixed state (white noise) and d is the dimension of ρ.

For the transpose operation T, the value of p is calculated by maximizing the fidelity between T and $\widetilde{T}$ operated on a

*foresttht@gmail.com
†Present address: Information Technology Laboratory, NIST, Gaithersburg, MD 20899, USA.
‡bae.joonwoo@gmail.com
§yoonho72@gmail.com

pure state $|\psi\rangle$,

$$F = \mathrm{tr}[T[|\psi\rangle\langle\psi|]\widetilde{T}[|\psi\rangle\langle\psi|]] = 2/(d+1), \tag{2}$$

and is given by $p = d/(d+1)$. In the case of a qutrit, $\widetilde{T}$ is therefore given by [5]

$$\widetilde{T} = \tfrac{1}{4}T + \tfrac{3}{4}D. \tag{3}$$

While useful in showing how much white noise needs to be added to turn T (which is nonphysical) into a physically realizable $\widetilde{T}$, the above equation itself is not useful in designing an experimental setup. Based on the conjecture that SPA to a positive map is entanglement breaking and thus can be implemented with measurement and preparation of quantum states [5], Eq. (3) can be rewritten into the following decomposition as discussed in Refs. [7,8,17]:

$$\widetilde{T}[\rho] = \sum_{k=1}^{9} \mathrm{tr}\left[\frac{1}{3}|v_k^*\rangle\langle v_k^*|\rho\right]|v_k\rangle\langle v_k|, \tag{4}$$

where the vectors $|v_k\rangle$ are defined as

$$|v_1\rangle = \frac{1}{\sqrt{2}}\begin{pmatrix}1\\ \omega\\ 0\end{pmatrix}, \quad |v_2\rangle = \frac{1}{\sqrt{2}}\begin{pmatrix}1\\ \omega^2\\ 0\end{pmatrix}, \quad |v_3\rangle = \frac{1}{\sqrt{2}}\begin{pmatrix}1\\ \omega^3\\ 0\end{pmatrix}, \quad |v_4\rangle = \frac{1}{\sqrt{2}}\begin{pmatrix}0\\ 1\\ \omega\end{pmatrix}, \quad |v_5\rangle = \frac{1}{\sqrt{2}}\begin{pmatrix}0\\ 1\\ \omega^2\end{pmatrix},$$
$$|v_6\rangle = \frac{1}{\sqrt{2}}\begin{pmatrix}0\\ 1\\ \omega^3\end{pmatrix}, \quad |v_7\rangle = \frac{1}{\sqrt{2}}\begin{pmatrix}\omega\\ 0\\ 1\end{pmatrix}, \quad |v_8\rangle = \frac{1}{\sqrt{2}}\begin{pmatrix}\omega^2\\ 0\\ 1\end{pmatrix}, \quad |v_9\rangle = \frac{1}{\sqrt{2}}\begin{pmatrix}\omega^3\\ 0\\ 1\end{pmatrix},$$

and this form of SPA-T can be directly implemented in the laboratory. Here, $\omega = \exp(i2\pi/3)$ is the relative phase between two occupied bases. Note that these are known as symmetric and informationally complete positive-operator-valued measures (SIC-POVM) [18].

The quantum operation described in Eq. (4) can be schematically shown in Fig. 1. For a given qutrit state ρ, measurement is performed with the measurement operator $M_k = |v_k^*\rangle\langle v_k^*|/3$, where $|v_k^*\rangle$ are complex conjugates of $|v_k\rangle$. Note that $\{M_k = |v_k^*\rangle\langle v_k^*|/3\}_{k=1}^9$ forms a complete measurement set. Whenever the measurement is successful (the success probability is $p_k = \mathrm{tr}[M_k\rho]$), the corresponding quantum state $|v_k\rangle\langle v_k|$ is prepared and sent out. In Fig. 1, each set of measurement-preparation operations is denoted as $\widetilde{T}_k$; there are nine such measurement-preparation operations which must occur randomly with equal probabilities. Thus, for a qutrit state ρ, applying SPA-T is equivalent to making a projection measurement in the basis $|v_k^*\rangle$ (must be randomly chosen among nine basis states), and when successful, preparing a corresponding quantum state $|v_k\rangle$ to transmit. SPA-T of a qutrit state ρ, $\widetilde{T}[\rho]$, can then be described as an incoherent mixture

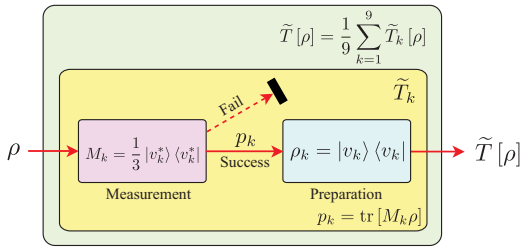

FIG. 1. (Color online) Scheme for implementing SPA-T for qutrit systems based on measurement and preparation of quantum states in Eq. (4). For an input qutrit state ρ, each operation $\widetilde{T}_k$ for $k = 1,\ldots,9$ is randomly applied with equal probability of 1/9. Then the output state becomes an equal mixture of the nine possibilities. Note that the probability for each $|v_k\rangle\langle v_k|$, p_k, is determined by the probability of successful outcome for the measurement M_k, i.e., $p_k = \mathrm{tr}[M_k\rho]$.

of nine states $|v_k\rangle\langle v_k|$ of which the probability of each state is determined by the corresponding measurement outcomes $\mathrm{tr}[M_k\rho]$ for $k = 1,\ldots,9$.

Let us now describe the linear optical implementation of the SPA-T described in Eq. (4). Photonic qutrit states are prepared using path (a and b) and polarization (horizontal H and vertical V) degrees of freedom of a single photon as shown in Fig. 2(a) [19,20]: $|0\rangle = |a,H\rangle$, $|1\rangle = |a,V\rangle$, and $|2\rangle = |b,H\rangle$ and the corresponding general qutrit states are described in Fig. 2(b). The single-photon source used in the experiment was prepared by using the spontaneous parametric down-conversion (SPDC) process in which a pair of 810-nm photons are generated in a 6-mm-thick type I β-BaB_2O_4 (BBO) crystal pumped with a 405-nm diode laser operating at 100 mW. The photon pairs propagate non-collinearly and detection of an idler photon at a trigger detector heralds preparation of a single-photon state for the signal photon [21]. An arbitrary single-photon qutrit state $|\psi\rangle = \alpha|0\rangle + \beta|1\rangle + \gamma|2\rangle$ where $|\alpha|^2 + |\beta|^2 + |\gamma|^2 = 1$ can then be prepared by using a set of wave plates (WP's) and a calcite beam displacer (BD); see Fig. 2(b). Note that the $|b,V\rangle$ state is never excited. The coincidence counting rate between the trigger detector and the detector counting the signal photon is approximately 18 kHz using interference filters with full width at half-maximum bandwidth of 10 nm and 5 nm for the signal and the idler photons, respectively.

The experimental setup for realizing SPA-T is shown in Fig. 2(c), where the whole setup consists of four parts: (i) state preparation, (ii) SPA measurement, (iii) SPA preparation, and (iv) quantum state tomography (QST). At the state preparation part, the initial single photon is transformed into an arbitrary qutrit state, $|\psi\rangle = \alpha|0\rangle + \beta|1\rangle + \gamma|2\rangle$. When the single-photon passes through BD1, which is 4.1-cm thick, the horizontally polarized component is refracted while the vertically polarized component is transmitted without refraction. The spatial separation between the two beams is 4.0 mm. By making use of the half-wave plate (HWP) in front of BD1, one can adjust the splitting ratio for upper path a_1 and lower path b_1, hence the amplitudes for $|0\rangle$ and $|2\rangle$. The HWP's

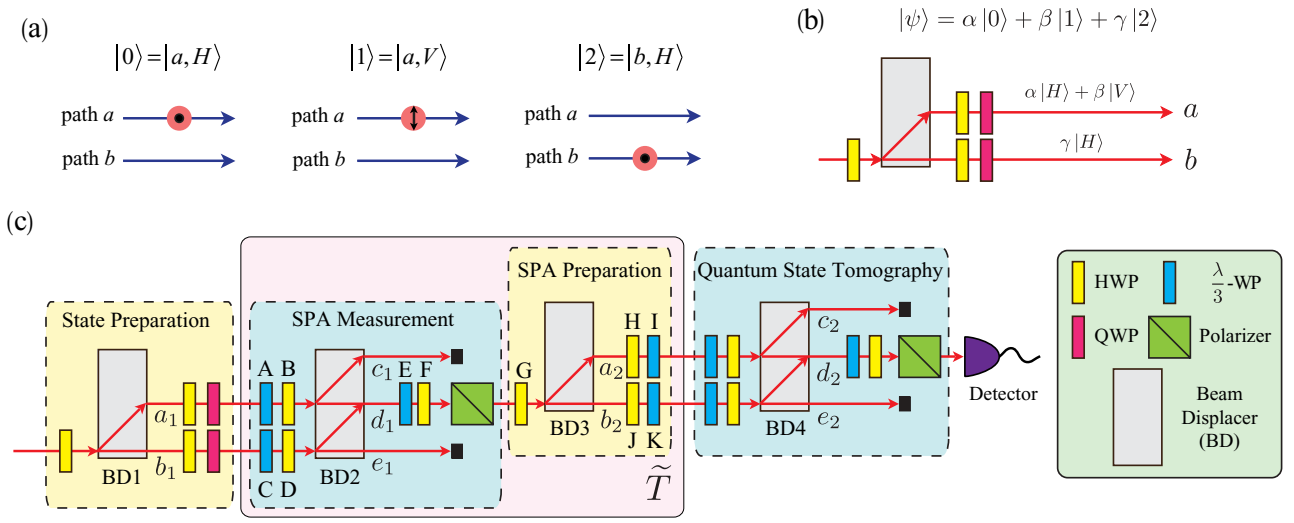

FIG. 2. (Color online) (a) Qutrit basis states are encoded on polarization (horizontal H and vertical V) and path (a and b) degrees of freedom of a single photon. Note that the $|b,V\rangle$ state is never excited. (b) Arbitrary single-photon qutrit states can be prepared by linear optics alone. BD splits horizontal and vertical polarization components spatially by 4 mm. (c) Experimental setup. The whole setup is composed of four parts: State preparation, SPA Measurement, SPA Preparation, and Quantum state tomography (QST). The SPA Measurement and SPA Preparation parts perform the approximate transpose operation $\widetilde{T}$ for the input state ρ. The $\lambda/3$-WP introduces the relative phase shift of $2\pi/3$ to the polarization component orthogonal to its fast axis. Angle settings for the labeled wave plates are shown in Table I.

and quarter-wave plates (QWP's) behind the BD1 are used for adjusting the ratio for horizontal and vertical polarizations, hence the amplitudes for $|0\rangle$ and $|1\rangle$, and for changing the relative phases among the three basis states.

At the SPA measurement part, an initial state ρ_{in} is projected to one of nine bases $|v_k^*\rangle$ with equal probability. Since the qutrit state is encoded in path and polarization degrees of freedom of a single photon, projection measurement on both degrees of freedom is needed and the measurement scheme is shown at the SPA measurement part in Fig. 2(c). In general, projection measurement for the path degree of freedom requires spatial interferometry (see Refs. [19,20]), while wave plates and a polarizer are needed for polarization measurement.

To describe the measurement scheme more in detail, first consider SPA measurement M_k for $k = 1,2,3$. In these cases, the measurement bases have equal ratios of $|0\rangle = |a_1,H\rangle$ and $|1\rangle = |a_1,V\rangle$ with different relative phases. Since the measurement bases have only $|a_1\rangle$ path component, projection measurement on the path degree of freedom is accomplished by directing the $|b_1\rangle$ component to one of the nondetecting output modes of BD2, e_1, using WP's (C and D) and BD2. For the polarization degree of freedom, projection measurement is accomplished by WP's (A and B) and BD2. Note that for the photon in the input path $|a_1\rangle$, BD2 functions as a polarizer, transmitting the vertically polarized component to the detecting output mode d_1 while the horizontally polarized component is directed to the nondetecting output mode c_1. A single photon (vertically polarized) found in mode d_1 signals successful SPA measurement. The remaining WP's (E and F) and the polarizer in mode d_1 are for other SPA measurements (k values other than 1,2,3) so the angles of the WP's (E and F) are set such that they do not alter the polarization state of the photon. See Table I for the angle settings of the WP's.

On the other hand, for $k = 4,5,6$, the measurement bases have an equal ratio of $|1\rangle = |a_1,V\rangle$ and $|2\rangle = |b_1,H\rangle$ with different relative phases. Unlike the cases of $k = 1,2,3$, the measurement bases have one component in each path $|a_1\rangle$ and $|b_1\rangle$. To perform the projection measurement onto these measurement bases, WP's (A and B) are first set so that $|0\rangle$

TABLE I. Angle settings of WP's, see Fig. 2(c), for each SPA measurement-preparation operation $\widetilde{T}_k$. The numbers represent counterclockwise rotation angles (in degrees) of the fast axes of WP's from the vertical polarization direction.

	A	B	C	D	E	F	G	H	I	J	K
$\widetilde{T}_1$	90°	22.5°	0°	45°	0°	0°	45°	67.5°	90°	45°	0°
$\widetilde{T}_2$	0°	22.5°	0°	45°	0°	0°	45°	67.5°	0°	45°	0°
$\widetilde{T}_3$	135	22.5°	0°	45°	0°	0°	45°	67.5°	45°	45°	0°
$\widetilde{T}_4$	90°	0°	0°	0°	0°	22.5°	22.5°	45°	0°	45°	0°
$\widetilde{T}_5$	90°	0°	0°	0°	90	22.5°	22.5°	45°	90°	45°	90°
$\widetilde{T}_6$	90°	0°	0°	0°	45°	22.5°	22.5°	45°	0°	45°	90°
$\widetilde{T}_7$	0°	45°	0°	0°	90	22.5°	22.5°	90°	0°	45°	90°
$\widetilde{T}_8$	0°	45°	0°	0°	0°	22.5°	22.5°	90°	90°	45°	0°
$\widetilde{T}_9$	0°	45°	0°	0°	45°	22.5°	22.5°	90°	0°	45°	0°

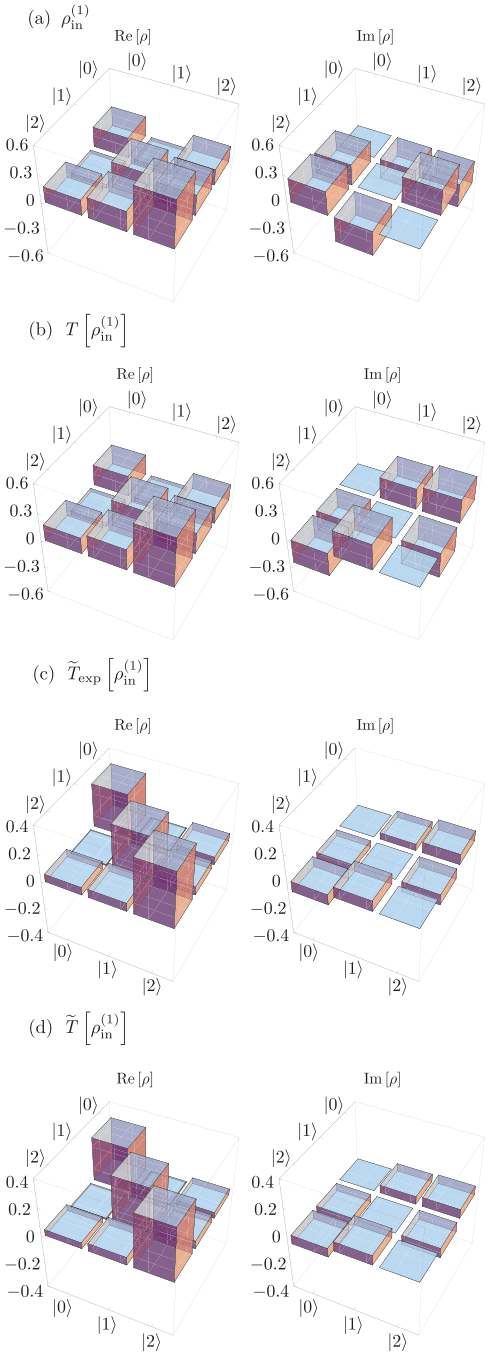

FIG. 3. (Color online) (a) QST of the input qutrit state $\rho_{\rm in}^{(1)}$. (b) Mathematically transposed state, $T[\rho_{\rm in}^{(1)}]$. (c) QST of the state after the experimentally implemented approximated transpose, $\widetilde{T}_{\rm exp}[\rho_{\rm in}^{(1)}]$. (d) The state after ideal approximated transpose, $\widetilde{T}[\rho_{\rm in}^{(1)}]$. Uhlmann's fidelity between (c) and (d) is $F \approx 0.999$.

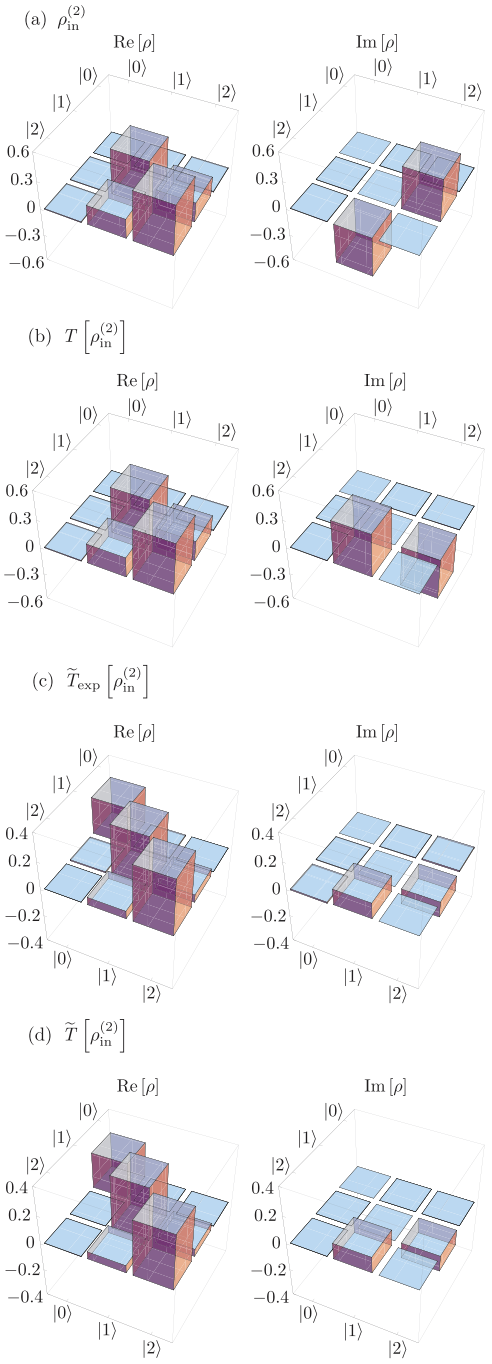

FIG. 4. (Color online) (a) QST of the input qutrit state $\rho_{\rm in}^{(2)}$. (b) Mathematically transposed state, $T[\rho_{\rm in}^{(2)}]$. (c) QST of the state after the experimentally implemented approximated transpose, $\widetilde{T}_{\rm exp}[\rho_{\rm in}^{(2)}]$. (d) The state after ideal approximated transpose, $\widetilde{T}[\rho_{\rm in}^{(2)}]$. Uhlmann's fidelity between (c) and (d) is $F \approx 0.999$.

component is directed to one of the nondetecting output modes, $|c_1\rangle$, as there is no projection onto the $|0\rangle = |a_1, H\rangle$ basis. At the same time, both $|1\rangle$ and $|2\rangle$ components are superposed at BD2 such that the following transformation occurs:

$$|1\rangle = |a_1, V\rangle \rightarrow |d_1, V\rangle \quad \text{and} \quad |2\rangle = |b_1, H\rangle \rightarrow |d_1, H\rangle$$

by using WP's (A $\sim$ D). The polarization projection measurement is then performed on the photon in mode d_1 in the basis $(\omega^k|H\rangle + |V\rangle)/\sqrt{2}$ where $\omega = \exp(i2\pi/3)$ by using WP's (E and F) and the polarizer. For $k = 7,8,9$, the measurement scheme is similar to that of $k = 4,5,6$ with the only difference being that $|1\rangle = |a_1, V\rangle$ is discarded instead of $|0\rangle = |a_1, H\rangle$. Actual angles settings for the WP's are shown in Table I.

For the initial qutrit state $\rho_{\rm in}$, the SPA measurement operation M_k has the success probability of $\langle v_k^*|\rho_{\rm in}|v_k^*\rangle$ and the polarization state of the photon after the SPA measurement

operation is $|V\rangle$ due to the projection at the polarizer. The SPA preparation operation then prepares the corresponding qutrit state $|v_k\rangle$ from $|V\rangle$ using WP's (G $\sim$ K) and BD3. Angle settings of WP's for the SPA preparation scheme are displayed in Table I.

In experiment, commercial zero-order HWP's and QWP's as well as custom-made $\lambda/3$-WP's, which introduce a relative phase difference of $2\pi/3$ between two orthogonal polarization components, were used for polarization state transformation. All WP's were mounted on motorized rotation stages for accurate and precise setting of the angles. As mentioned earlier, projection measurement for the path degree of freedom of a single-photon requires the formation of an interferometer [19,20]. For instance, BD1 and BD2 (also BD3 and BD4) form a Mach-Zehnder–type two-beam interferometer which needs to be stabilized. In our work, due to the compact design of the setup, the relative phase differences between the upper-lower paths (i.e., $a_1 - -b_1$ and $a_2 - -b_2$) were easily maintained over a day without any active feedback. Fine adjustment of the relative phase difference was achieved by horizontally tilting BD2 (BD4): We set the relative phase difference to 0 modulo 2π.

The output of the SPA measurement-preparation operation, which is a probabilistic sum of nine equally weighted $\widetilde{T}_k$ operations, then corresponds to the SPA-T operation $\widetilde{T}_{\rm exp}[\rho_{\rm in}]$. To confirm that the SPA-T operation has indeed been accomplished, we carry out QST to reconstruct the experimental output state $\widetilde{T}_{\rm exp}[\rho_{\rm in}]$ and compare it with the ideal SPA-T operation $\widetilde{T}[\rho_{\rm in}]$ [22,23]. In general, for d-dimensional quantum states, i.e, qudits, at least d^2 different measurements are required to fully reconstruct the state. To perform QST on a qutrit state, we used $\{|v_k\rangle\langle v_k|\}_{k=1}^{9}$ as a set of nine QST measurement bases [18,24]. The angles setting of the WP's for the QST measurement basis $|v_k\rangle\langle v_k|$ can be found in Table I. Note that $|v_1\rangle = |v_2^*\rangle$, $|v_2\rangle = |v_1^*\rangle$, $|v_3\rangle = |v_3^*\rangle$, etc. In addition, in order to confirm that the experimentally implemented SPA-T operation is performed well, we have also carried out quantum process tomography (QPT) [25]. QST and QPT results were obtained using the maximum likelihood estimation method [22,25].

In order to graphically show how SPA-T transforms a qutrit state, we show the results for two input states $\rho_{\rm in}^{(1)}$ and $\rho_{\rm in}^{(2)}$ among the variety of input states that we tested. The experimentally prepared input state $\rho_{\rm in}^{(1)}$ is identified by QST and the density matrix of this input state is shown in Fig. 3(a). The qutrit state $\rho_{\rm in}^{(1)}$ was chosen for a clear demonstration of the state transformation (in the computational basis) due to the SPA-T operation as all off-diagonal elements are nonzero. The transposed state of the input state can be obtained as $T[\rho_{\rm in}^{(1)}]$ which is represented in Fig. 3(b). Notice that the real part of the density matrix (Re$[\rho]$) remains without any change but the off-diagonal terms in the imaginary part of the density matrix (Im$[\rho]$) are interchanged. This is due to the Hermitian property of the density matrix. Then, the resultant state $\widetilde{T}_{\rm exp}[\rho_{\rm in}^{(1)}]$ after the experimentally realized SPA-T operation is shown in Fig. 3(c). Compared to the input state $\rho_{\rm in}^{(1)}$, the amplitudes of the off-diagonal terms in $\widetilde{T}_{\rm exp}[\rho_{\rm in}^{(1)}]$ are decreased and the magnitude differences among diagonal terms are reduced due to the effect of mixing with a white noise. One can also easily notice that the off-diagonal terms in imaginary parts are interchanged like the transposed state. Assuming the ideal SPA-T operation, the output state would be $\widetilde{T}[\rho_{\rm in}^{(1)}]$ and is represented in Fig. 3(d). To quantify the performance of the realized operation, we evaluate Uhlmann's fidelity $F(\rho,\sigma) = [{\rm tr}\sqrt{\sqrt{\rho}\sigma\sqrt{\rho}}]^2$ between two states, one from the experimental realization $\rho = \widetilde{T}_{\rm exp}[\rho_{\rm in}]$ and the other from the ideal one $\sigma = \widetilde{T}[\rho_{\rm in}]$ [26]. Our experimental results show $F(\widetilde{T}_{\rm exp}[\rho_{\rm in}^{(1)}], \widetilde{T}[\rho_{\rm in}^{(1)}]) \approx 0.999$.

The reconstructed density matrix of another experimentally prepared input state $\rho_{\rm in}^{(2)}$ is graphically shown in Fig. 4(a). The qutrit state $\rho_{\rm in}^{(2)}$ was specifically chosen to demonstrate the effect of admixing with white noise. Similarly to the results for $\rho_{\rm in}^{(1)}$, the density matrices of $T[\rho_{\rm in}^{(2)}]$, $\widetilde{T}_{\rm exp}[\rho_{\rm in}^{(2)}]$, and $\widetilde{T}[\rho_{\rm in}^{(2)}]$ are represented in Figs. 4(b), 4(c), and 4(d), respectively. Note that although the initial state $\rho_{\rm in}^{(2)}$ has almost no components in the $|0\rangle$ basis, $\widetilde{T}_{\rm exp}[\rho_{\rm in}^{(2)}]$ has $|0\rangle$ basis component due to the mixing with a white noise. The obtained fidelity value is $F(\widetilde{T}_{\rm exp}[\rho_{\rm in}^{(2)}], \widetilde{T}[\rho_{\rm in}^{(2)}]) \approx 0.999$. We also repeated SPA-T to a few more states, and the obtained values of fidelities are higher than 0.989.

The experimentally realized SPA-T operation can be identified with QPT. In general, for a quantum operation on a

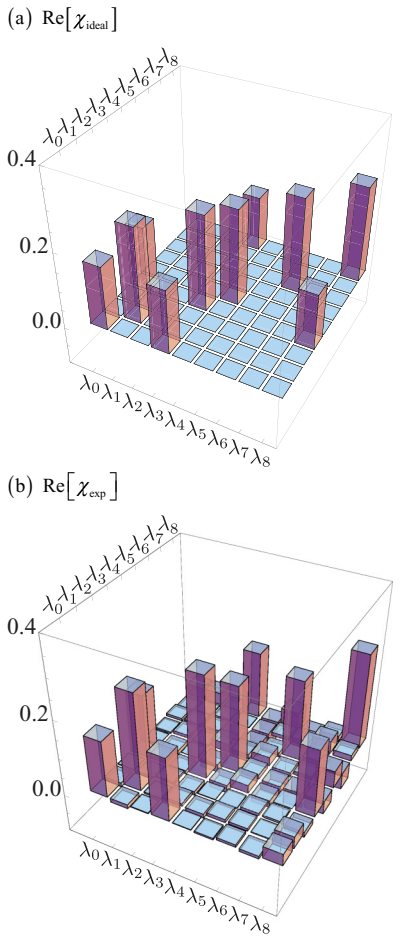

FIG. 5. (Color online) (a) The QPT matrix $\chi_{\rm ideal}$ for the ideal SPA transpose operation $\widetilde{T}$. (b) The QPT matrix $\chi_{\rm exp}$ for the implemented SPA-T operation $\widetilde{T}$. Note that only the real parts of the χ matrices are shown, as the imaginary parts are almost zero. The average fidelity between the ideal and realized operations is $F_{\rm ave}(\widetilde{T}, \widetilde{T}_{\rm exp}) \approx 0.982$.

d-dimensional quantum system, d^2 different input states are required to carry out QPT and one needs to analyze the state before and after the realized operation using QST for each input state. A quantum process ε of a single qudit can generally be expressed as

$$\varepsilon(\rho_{\rm in}) = \sum_{m,n=0}^{d^2-1} \chi_{m,n}\, \lambda_m\, \rho_{\rm in}\, \lambda_n^{\dagger}, \tag{5}$$

where $\{\lambda_m\}_{m=0}^{d^2-1}$ forms the complete set of $d \times d$ dimensional operator basis and the process matrix χ gives the complete characterization of the operation ε. Note that χ is a $d^2 \times d^2$ matrix.

If one chooses a certain basis set $\{\lambda_m\}_{m=0}^{d^2-1}$, the process matrix χ is uniquely determined, and by performing QST, χ can be experimentally identified. For a single-qutrit system, nine operator bases are needed, and we used the following as the complete operator basis set [23]:

$$\lambda_0 = \begin{pmatrix} 1 & 0 & 0 \\ 0 & 1 & 0 \\ 0 & 0 & 1 \end{pmatrix}, \quad \lambda_1 = \begin{pmatrix} 0 & 1 & 0 \\ 1 & 0 & 0 \\ 0 & 0 & 0 \end{pmatrix}, \quad \lambda_2 = \begin{pmatrix} 0 & -i & 0 \\ i & 0 & 0 \\ 0 & 0 & 0 \end{pmatrix}, \quad \lambda_3 = \begin{pmatrix} 1 & 0 & 0 \\ 0 & -1 & 0 \\ 0 & 0 & 0 \end{pmatrix}, \quad \lambda_4 = \begin{pmatrix} 0 & 0 & 1 \\ 0 & 0 & 0 \\ 1 & 0 & 0 \end{pmatrix},$$

$$\lambda_5 = \begin{pmatrix} 0 & 0 & -i \\ 0 & 0 & 0 \\ i & 0 & 0 \end{pmatrix}, \lambda_6 = \begin{pmatrix} 0 & 0 & 0 \\ 0 & 0 & 1 \\ 0 & 1 & 0 \end{pmatrix}, \quad \lambda_7 = \begin{pmatrix} 0 & 0 & 0 \\ 0 & 0 & -i \\ 0 & i & 0 \end{pmatrix}, \quad \lambda_8 = \frac{1}{\sqrt{3}} \begin{pmatrix} 1 & 0 & 0 \\ 0 & 1 & 0 \\ 0 & 0 & -2 \end{pmatrix},$$

where one can easily notice that λ_0 is an identity operator.

The ideal process matrix $\chi_{\rm ideal}$ for SPA-T is given as

$$\chi_{\rm ideal} = \begin{pmatrix} \frac{1}{6} & 0 & 0 & \frac{1}{6} & 0 & 0 & 0 & 0 & 0 \\ 0 & \frac{1}{4} & 0 & 0 & 0 & 0 & 0 & 0 & 0 \\ 0 & 0 & 0 & 0 & 0 & 0 & 0 & 0 & 0 \\ \frac{1}{6} & 0 & 0 & \frac{1}{4} & 0 & 0 & 0 & 0 & \frac{1}{4\sqrt{3}} \\ 0 & 0 & 0 & 0 & \frac{1}{4} & 0 & 0 & 0 & 0 \\ 0 & 0 & 0 & 0 & 0 & 0 & 0 & 0 & 0 \\ 0 & 0 & 0 & 0 & 0 & 0 & \frac{1}{4} & 0 & 0 \\ 0 & 0 & 0 & 0 & 0 & 0 & 0 & 0 & 0 \\ 0 & 0 & 0 & \frac{1}{4\sqrt{3}} & 0 & 0 & 0 & 0 & \frac{1}{4} \end{pmatrix},$$

and the above $\chi_{\rm ideal}$ is graphically shown in Fig. 5(a). The process matrix for the performed operation is experimentally constructed by QPT, and the experimentally reconstructed process matrix $\chi_{\rm exp}$ is shown in Fig. 5(b). The average fidelity between the ideal and the realized operation is calculated to be $F_{\rm ave}(\widetilde{T}, \widetilde{T}_{\rm exp}) = \int d\psi\, F(\widetilde{T}[|\psi\rangle\langle\psi|], \widetilde{T}_{\rm exp}[|\psi\rangle\langle\psi|]) \approx 0.982$. We believe that the small discrepancy between the ideal and realized operations is mainly caused by slight misalignment of the relative phase difference in the interferometers formed by BD1-BD2 and BD3-BD4 in Fig. 2. For detailed discussions on the gate fidelity related to nonunitary operations, see Ref. [27].

In summary, we have reported a linear optical experimental realization of the approximate transpose operation for a photonic qutrit system. Our scheme is based on the conjecture that SPA to a positive map is entanglement breaking, so the SPA scheme is built upon measurement and preparation of quantum states. Our work demonstrates that SPA's for high-dimensional quantum systems can be realized in experiment within the present-day technology. Furthermore, our work on SPA-T paves the way toward entanglement detection based on SPA-PT for high-dimensional quantum systems.

This work was supported in part by the National Research Foundation of Korea (Grants No. 2011-0021452 and No. 2012-002588). H.T.L. acknowledges support from the National Junior Research Fellowship (Grant No. 2012-000642). J.B. acknowledges support from the National Research Foundation and Ministry of Education, Singapore.

[1] A. Peres, Phys. Rev. Lett. **77**, 1413 (1996).
[2] M. Horodecki, P. Horodecki, and R. Horodecki, Phys. Lett. A **223**, 1 (1996).
[3] Note that not all entangled states give rise to a negative eigenvalue after partial transpose. Bound entanglement is such an example.
[4] P. Horodecki and A. Ekert, Phys. Rev. Lett. **89**, 127902 (2002).
[5] J. K. Korbicz, M. L. Almeida, J. Bae, M. Lewenstein, and A. Acin, Phys. Rev. A **78**, 062105 (2008).
[6] M. Horodecki, P. W. Shor, and M. B. Ruskai, Rev. Math. Phys. **15**, 629 (2003).
[7] H.-T. Lim, Y.-S. Ra, Y.-S. Kim, J. Bae, and Y.-H. Kim, Phys. Rev. A **83**, 020301(R) (2011).
[8] H.-T. Lim, Y.-S. Kim, Y.-S. Ra, J. Bae, and Y.-H. Kim, Phys. Rev. Lett. **107**, 160401 (2011).
[9] C. M. Alves, P. Horodecki, D. K. L. Oi, L. C. Kwek, and A. K. Ekert, Phys. Rev. A **68**, 032306 (2003).
[10] A. V. Burlakov, M. V. Chekhova, O. A. Karabutova, D. N. Klyshko, and S. P. Kulik, Phys. Rev. A **60**, R4209 (1999).
[11] A. Mair, A. Vaziri, G. Weihs, and A. Zeilinger, Nature (London) **412**, 313 (2001).
[12] D. Collins, N. Gisin, N. Linden, S. Massar, and S. Popescu, Phys. Rev. Lett. **88**, 040404 (2002).
[13] Y. I. Bogdanov *et al.*, Phys. Rev. Lett. **93**, 230503 (2004).
[14] R. T. Thew, A. Acin, H. Zbinden, and N. Gisin, Phys. Rev. Lett. **93**, 010503 (2004).

[15] S.-Y. Baek, S. S. Straupe, A. P. Shurupov, S. P. Kulik, and Y.-H. Kim, Phys. Rev. A **78**, 042321 (2008).
[16] A. C. Dada, J. Leach, G. S. Buller, M. J. Padgett, and E. Andersson, Nat. Phys. **7**, 677 (2011).
[17] J. Bae (in preparation).
[18] J. M. Renes, R. Blume-Kohout, A. J. Scott, and C. M. Caves, J. Math. Phys. **45**, 2171 (2004).
[19] Y.-H. Kim, Phys. Rev. A **67**, 040301(R) (2003).
[20] S.-Y. Baek and Y.-H. Kim, Phys. Lett. A **375**, 3834 (2011).
[21] Y.-S. Kim, H.-T. Lim, Y.-S. Ra, and Y.-H. Kim, Phys. Lett. A **374**, 4393 (2010).
[22] D. F. V. James, P. G. Kwiat, W. J. Munro, and A. G. White, Phys. Rev. A **64**, 052312 (2001).
[23] R. T. Thew, K. Nemoto, A. G. White, and W. J. Munro, Phys. Rev. A **66**, 012303 (2002).
[24] Z. E. D. Medendorp, F. A. Torres-Ruiz, L. K. Shalm, G. N. M. Tabia, C. A. Fuchs, and A. M. Steinberg, Phys. Rev. A **83**, 051801(R) (2011).
[25] J. Fiurasek and Z. Hradil, Phys. Rev. A **63**, 020101(R) (2001).
[26] A. Uhlmann, Rep. Math. Phys. **9**, 273 (1976).
[27] H.-T. Lim, Y.-S. Ra, Y.-S. Kim, Y.-H. Kim, and J. Bae, arXiv:1106.5873v1.